Article

Divergence in Antiviral Activities of Carbon Dots versus Nano-Carbon/Organic Hybrids and Implications

Cristian E. Rodriguez [1], Audrey F. Adcock [1], Buta Singh [2], Subhadra Yerra [2], Yongan Tang [3], Ya-Ping Sun [2,*] and Liju Yang [1,*]

1 Department of Pharmaceutical Sciences, Biomanufacturing Research Institute and Technology Enterprise, North Carolina Central University, Durham, NC 27707, USA
2 Department of Chemistry, Clemson University, Clemson, SC 29634, USA
3 Department of Mathematics and Physics, North Carolina Central University, Durham, NC 27707, USA
* Correspondence: syaping@g.clemson.edu (Y.-P.S.); lyang@nccu.edu (L.Y.)

Abstract: Carbon dots (CDots) are generally defined as small carbon nanoparticles (CNPs) with effective surface passivation, for which the classical synthesis is the functionalization of pre-existing CNPs with organic molecules. However, "dot" samples produced by "one-pot" thermal carbonization of organic precursors are also popular in the literature. These carbonization-produced samples may contain nano-carbon domains embedded in organic matters from the precursors that survived the thermal processing, which may be considered and denoted as "nano-carbon/organic hybrids". Recent experimental evidence indicated that the two different kinds of dot samples are largely divergent in their photo-induced antibacterial functions. In this work, three representative carbonization-produced samples from the precursor of citric acid–oligomeric polyethylenimine mixture with processing conditions of 200 °C for 3 h (CS200), 330 °C for 6 h (CS330), and microwave heating (CS$_{MT}$) were compared with the classically synthesized CDots on their photo-induced antiviral activities. The results suggest major divergences in the activities between the different samples. Interestingly, CS$_{MT}$ also exhibited significant differences between antibacterial and antiviral activities. The mechanistic origins of the divergences were explored, with the results of different antimicrobial activities among the hybrid samples rationalized in terms of the degree of carbonization in the sample production and the different sample structural and morphological characteristics.

Keywords: carbon dots; nano-carbon/organic hybrids; thermal carbonization; photoinduced antiviral function
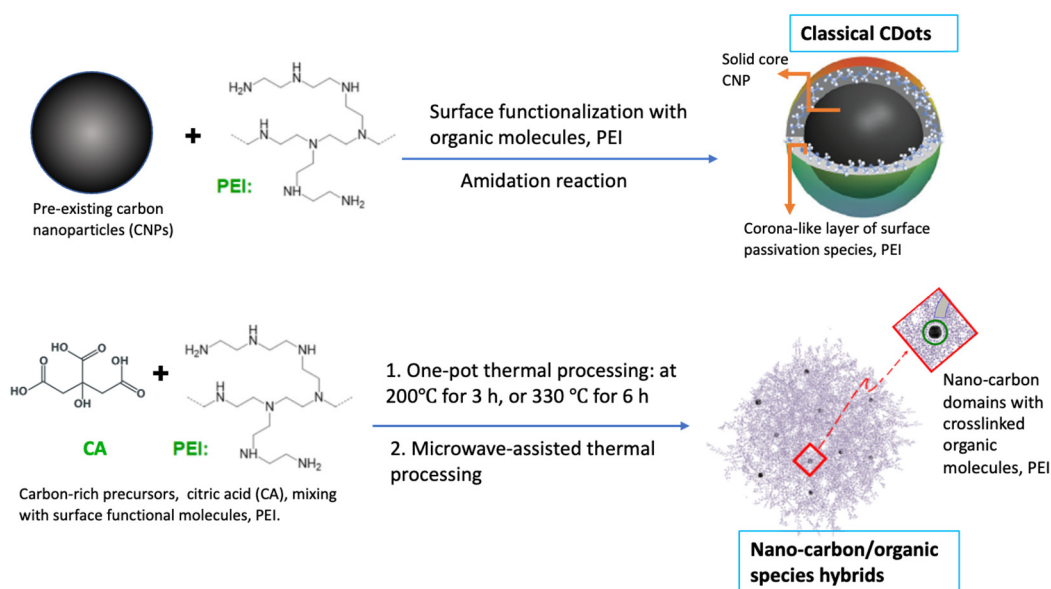
1. Introduction

Carbon dots (CDots) are generally defined as small carbon nanoparticles (CNPs) of "core-shell" like nanostructures, each with a CNP core (<10 nm in diameter) and a thin shell of organic molecules for surface passivation [1–3]. CDots have recently been recognized as a new class of photoactive nanomaterials that can be activated by visible light to exhibit excellent antimicrobial activities against a broad range of microbials, including bacteria and viruses. Since our first report on CDots as potent antibacterial agents under visible/natural light against model Gram-positive and Gram-negative bacteria such as *Bacillus subtilis* and *Escherichia coli* [4], subsequent strong experimental results have consistently proven that CDots and derived hybrid dots possess excellent photo-activated antibacterial and antiviral functions [5–14].

Mechanistically, the visible light-activated antimicrobial activity is attributed to the combined actions of two types of reactive species that are formed in the photoexcited states of CDots. Upon photoexcitation of CDots, there must be rapid charge transfers and separation to form electrons and holes trapped separately in various surface defect sites of the CNP core, which are stabilized by the organic surface passivation. These initially separated redox pairs are highly potent in their antimicrobial activities. The radiative

recombination of the redox pairs results in the formation of longer-lived emissive excited states, which are responsible for the observed colorful fluorescence emissions, as well as for the generation of classical reactive oxygen species (ROS). The separated redox pairs and the classical ROS collectively contribute to the observed excellent antimicrobial outcomes with light-activated CDots [7,10,12,13].

As defined, CDots can be prepared via surface functionalization of pre-existing CNPs with selected organic molecules (Figure 1), such as oligomeric polyethylenimine (PEI) for PEI-CDots of benchmark antimicrobial performance [7,10]. However, a large volume of reported studies in the literature have been based on "dot" samples obtained via thermal or hydrothermal processing of selected organic precursors [1,15–32], such as the frequently used mixtures of citric acid (CA) with PEI [33–39] and other carbon-rich precursors [40–46], under different processing conditions for their carbonization to create nano-carbon entities or domains mimicking CNPs. Structurally, in the samples thus produced, there are domains in which the nano-carbon entities created via carbonization are locally surrounded by the organic species that have survived the carbonization processing conditions, in a configuration somewhat analogous to that of the CNPs surface passivated by organic functionalization in the definition of CDots [1]. The available experimental results have suggested that the nanoscale domains are crosslinked by abundant organic species in such samples, so that the carbonization-produced dot samples are more appropriately characterized and denoted as "nano-carbon/organic hybrids" (Figure 1) [29,47].

Figure 1. Illustration of the synthesis route of the classical CDots (PEI-CDots as a specific example prepared by the functionalization of pre-existing CNPs with PEI, oligomeric polyethylenimine, as surface passivation molecules) and that of the "nano-carbon/organic hybrids" prepared from the thermal processing of selected organic precursors (mixtures of CA and PEI as the specific example used in this study) under different processing conditions.

The similarity in configuration between the nanoscale domains in nano-carbon/organic hybrids and classical CDots may be credited for their partially comparable optical spectroscopic properties, including the characteristic excitation wavelength-dependent fluorescence emissions [29,47,48]. However, there is clearly significant divergence between the hybrids and classical CDots in terms of their antibacterial functions [48]. For example, as found in our previously reported study [48], the carbonization produced samples with mixtures of CA and PEI, as precursors illustrated in Figure 1 were all less effective than PEI-CDots in antibacterial activities under visible light, which was attributed to the majorly different sample morphologies affecting interactions with the targeted bacterial species.

In this work, the same hybrid samples and PEI-CDots with visible light exposure were compared in terms of their antiviral activities against vesicular stomatitis virus (VSV), an enveloped, negative-sense RNA virus, as a representative virus target. There was still divergence among the hybrids (Figure 1) versus the classical CDots, but the divergence was somewhat different from that in their antibacterial activities. The results are discussed in terms of different structures and compositions in these dot samples, and their mechanistic implications are also discussed.

2. Materials and Methods

2.1. Synthesis of Dots Samples

Citric acid (CA) was purchased from Alfa Aesar (Tewksbury, MA, USA), and oligomeric polyethylenimine (PEI, branched, average molecular weight ~600) from Polysciences, Inc. (Warrington, PA, USA). Dialysis membrane tubing (molecular weight cut-off ~500 or ~1000) was supplied by Spectrum Laboratories. Water was deionized and purified by passing through a Labconco WaterPros water purification system (Labconco, Kansas City, MO, USA).

CS200 and CS330 samples were synthesized using CA–PEI mixture as a precursor for thermal progressing at 200 °C for 3 h and at 330 °C for 6 h, respectively. The CS_{MT} sample was prepared from the same precursor mixture; the heating took place in a conventional microwave oven. The as-prepared samples were cleaned via dialysis in membrane tubing (molecular weight cut-off ~1000) against fresh water to obtain colored aqueous solutions. Detailed information and processes for the synthesis and post-synthesis treatments for these samples have been reported [48], and copies of the protocols with references can be found in the Supplementary Materials.

PEI-CDots were prepared via surface functionalization of small carbon nanoparticles with oligomeric polyethylenimine (PEI, average molecular weight ~600, branched). The small carbon nanoparticles were obtained from a commercially acquired carbon nano-powder sample, which was treated via refluxing in concentrated nitric acid, followed by dialysis and dispersion in aqueous solution. The PEI functionalization of the nanoparticles was achieved during the microwave-assisted thermal processing. Details on the preparation and characterization of PEI-CDots were reported previously [49,50]. Copies of the synthesis protocol with references are provided as Supplementary Materials.

The characterization results on the structural and optical properties of the dot samples, including atomic force microscopy (AFM) imaging results, UV/vis absorption spectra, fluorescence emission spectra and excitation wavelength dependencies, and the fluorescence quenching by an electron donor and acceptor analyzed in terms of Stern–Volmer plots, were reported previously [48].

2.2. VSV Virus Propagation and Purification, and Virus Titration by the Plaque Assay

VSV, Indiana strain (VR-1238), and baby hamster kidney (BHK-21) cells (CCL-10) were purchased from ATCC (Manassas, VA, USA). VSV was propagated in confluent monolayers of BHK-21 cells. Viruses were harvested approximately 18 h post inoculation, followed by purification steps, and then resuspended in 2 mL of sterile deionized (DI) H_2O for stock. The protein concentration was determined based on the spectrophotometric measurement, and the final protein concentration of the VSV sample was set at 1 µg/mL. The purified VSV samples were stored at refrigeration until the viral titer was determined by the plaque assay and for further experimental uses.

The VSV titer was quantified using the plaque assay in BHK-21 cells. Briefly, BHK-21 cells were seeded into six-well plates at a density of ~1×10^6 cells/well and incubated overnight to form confluent cell monolayers. The VSV samples were 1:10 serially diluted with Dulbecco's Modified Eagle Medium (DMEM), and aliquots of 400 µL of the dilution series were added to inoculate the BHK-21 cell monolayers. After overnight incubation, the cells were fixed with 4% formaldehyde solution and stained with 0.05% crystal violet in 20% methanol for plaque visualization and counting. The plaque number was calculated into the

plaque-forming units per mL (PFU/mL) for the viral titer. More detailed protocols of VSV propagation and purification, and the plaque assay for viral titration were reported in our previous study [13], and copies of the detailed protocols are provided in the Supplementary Materials.

2.3. Dots Treatment for VSV Inactivation

All dots treatments for VSV viruses were carried out in 96-well plates using the protocol reported in our previous study [13], with modifications. Briefly, for dose dependent tests, aliquots of 100 µL of purified VSV particles at stock concentration in high 10^9 PFU/mL were mixed with desired volumes of dot samples to the final VSV concentration at low 10^9 PFU/mL and the final dot concentrations ranging from 10 to 200 µg/mL, in a total volume of 150 µL in each well, were adjusted by adding sterile DI H_2O. Control samples of VSVs in sterile DI H_2O without any dot sample were also included in each experiment. The samples of treatment at each dot concentration were prepared in duplicates. Another plate prepared in the same way was wrapped in aluminum foil to block light and used as the control for the dot treatment in the dark condition. Both plates were placed on an Orbital shaker (BT Lab Systems) with shaking at 330 rpm and exposed to visible light from a commercially acquired household daylight light-emitting diode (LED) bulb using CREE (omnidirectional 815 lumens, 5000 K) (purchased from Home Depot) placed at ~10 cm above the surface of the plates for 1 h. The light intensity on the samples was determined using a power meter (Edmund Optics Inc., Barrington, NJ, USA) and was ~7.8 mW/cm^2. After the treatments (which were stopped by restricting light exposure), each treated and control sample was immediately 1:10 serially diluted with DMEM. The viral titer in each sample was determined using the plaque assay described above. Control samples without VSVs but with dots concentrations equivalent to those in the serial dilutions were included as cytotoxicity controls to make sure CDots had no effect on the BHK-21 host cells. For all dots treatment experiments, at least three independent tests were performed. The dose concentration-dependent inactivation curve of VSVs for each different dot sample was plotted according to the logarithmic value of virus titer in PFU/mL vs. the dot concentration.

2.4. Determination of ROS Generation during Dot Treatment to VSVs

The 2',7'-dichlorodihydrofluorescein diacetate (H_2DCFDA) (Molecular Probes, Eugene, OR) was used as the fluorescence probe for the determination of total reactive oxygen species (ROS) generation during dot treatment to VSVs. Briefly, VSVs were treated with dot samples at 50 and 100 µg/mL using the same protocol as described above, but they were modified to use 48 wells with a total volume of 400 µL. After treatment, for each treatment and control sample, aliquots of 200 µL VSVs samples were placed into the wells of a black 96-well plate in replicates. Then, aliquots of 2 µL of 1 mM H_2DCFDA were added to one of the replicated wells and the same volume of PBS was added to the second replicate of each treatment. The plate was placed on the plate shaker for mixing for 30 s, then incubated in a cell culture incubator for 30 min. After incubation, the fluorescence intensity of each well was read on the SpectraMax M5 plate reader with the 485 nm/528 nm filter. The net fluorescence intensity of each sample was calculated using the RFU of the sample with H_2DCFDA, subtracting the RFU of the counter sample without H_2DCFDA. The fold of ROS increase was calculated using the net fluorescence intensity of each treated sample divided by the net fluorescence intensity of the control VSV sample without dot treatment.

3. Results and Discussion

3.1. Similarities and Differences in Optical Spectroscopic Properties and Structural Features of CDots and Nano-Carbon/Organic Hybrids

In our earlier study [48], we identified similarities and differences in optical spectroscopic properties between classical CDots and the carbonization-produced hybrid samples, as well as among the hybrid samples prepared under different conditions. All the hy-
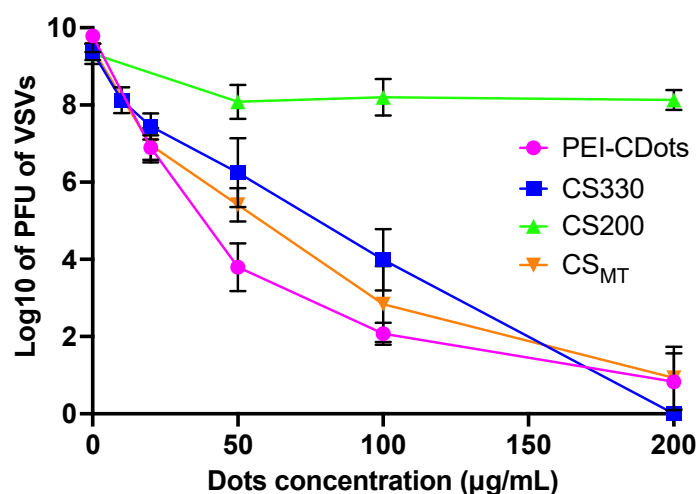
brid samples in aqueous solutions (CS200, CS330, and CS_{MT}) are absorptive in visible wavelengths, with similar absorption spectra comparable to that of the PEI-CDots, but significantly different in absorbances due to the different nano-carbon contents in the samples. CS300 and CS_{MT} are similar to PEI-CDots with strong absorptions in the visible spectrum (400 nm and longer wavelengths), but CS200 is only weakly absorptive over the same visible spectral region. The correspondingly much lower nano-carbon content in CS200 than those in CS300 and CS_{MT} is due to the too-mild thermal processing conditions for CS200. However, all hybrid samples are fluorescent, and their fluorescence spectral profiles at the same wavelength of excitation (400 nm, for example) are largely similar among themselves and also similar to that of PEI-CDots. The similarities in the optical spectroscopic properties of these samples are indicative of their shared photon harvesting abilities over the visible spectrum, which are necessary to drive the antimicrobial activities, and suggest some similar processes and characteristics in the photoexcited states of these materials.

In terms of sample structures, however, the available experimental results generally confirm the expectation that classical CDots like PEI-CDots are individual dots, each with a preexisting carbon nanoparticle core and a corona-like surface layer of organic functionalization species [29], and the hybrid samples are composed of nano-carbon domains immersed in organic materials derived from the organic precursors due to the thermal processing conditions intended for carbonization. The sample structural similarities between classical CDots and hybrid samples and also among the different hybrid samples are such that they all contain the configuration of nano-carbon surrounded by organic species, with a length scale of such configuration roughly at ten or tens of nanometers, which is much shorter than the wavelengths in the optical absorption and fluorescence emission spectra. Consequently, as far as the optical spectroscopic properties are concerned, the sample structural differences are non-existent (because again, the differences are at a much shorter length scale than the light wavelengths). However, the sample structures do matter with respect to the antimicrobial activities of the photo-generated reactive species in the different dot samples because of the generally short or ultra-short lifetimes of the reactive species. The significantly different antibacterial activities and outcomes of the different dot samples upon visible light excitation were investigated and reported [48]. In this work on the light-activated antiviral properties of the different dot samples, the same kinds of similarities and more divergences were found.

3.2. Photo-Activated Antiviral Activities of CDots vs. Nano-Carbon/Organic Hybrids

The visible light-activated antiviral activities of the CS200, CS330, and PEI-CDots toward VSVs were compared. In the experiments, VSVs in suspension ($\sim10^9$ PFU/mL) were treated with hybrids and PEI-CDots at concentrations ranging from 10 to 200 μg/mL and with visible light exposure for 1 h for inactivation, along with the VSVs samples without any dots as controls. After the treatments, the virus titers in the treated samples and the control samples were determined based on the plaque assay. The dose–response curve of VSVs in response to each of the tested dot samples is plotted in terms of the logarithmic virus titer against the concentration of individual nano-carbon/organic hybrids samples and PEI-CDots used in the treatments (Figure 2). As shown in Figure 2, clearly, the CS200 sample lacked the light-activated antiviral function, while the CS330 sample could inactivate VSVs, but was significantly less effective than PEI-CDots at low concentrations. At sufficiently high concentrations ($\geq$200 μg/mL), the inactivation of VSVs (10^9 PFU/mL) using the CS330 sample was close to complete, similar to that involving PEI-CDots. The CS_{MT} sample also exhibited significant antiviral activity against VSVs, with the performance generally in between those of the CS330 sample and PEI-CDots (Figure 2).
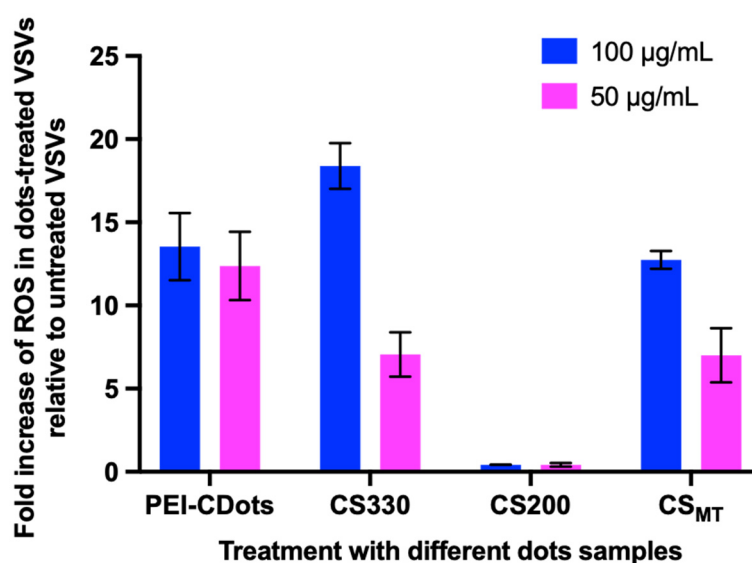
Figure 2. The dose-dependent antiviral activities of CS200, CS330, CS_{MT}, and PEI-CDots with visible-light exposure (all for 1 h) against VSVs, expressed by the reduction in $\log_{10}$ of viral titers with increasing concentrations of the hybrids and PEI-CDots used in the treatments.

The relative antiviral activity of the PEI-CDots and the three carbonization-produced samples clearly shows that PEI-CDots is significantly more effective, which is in general agreement with the previously reported results on the relative antibacterial activity comparison between these samples [48], except for the CS_{MT} sample. In the antibacterial activity results, CS330 showed significantly reduced antibacterial activity compared to that of PEI-CDots, whereas CS200 and CS_{MT} showed no antibacterial activity [48] (Detailed information is provided in Supplementary Materials Figure S1). A rationalization of the results is such that the relative antiviral activities of these hybrids samples are most likely correlated with the degree of carbonization in the samples due to the different thermal processing conditions in their syntheses [47,48,51]. More specifically, the processing condition of 200 °C for 3 h for the CS200 sample was much too mild to achieve the intended carbonization, hence the lack of content of nano-carbon domains in the sample and the apparent lack of photo-activated antiviral activity. For the CS330 sample, processing at 330 °C for 6 h was more appropriate for the desired carbonization to result in more defined nano-carbon domains in the sample [48,51], which were responsible for the more potent photo-activated antiviral activity. The CS_{MT} sample exhibited antiviral activity between those of the CS330 sample and PEI-CDots, consistent with the anticipated more significant carbonization associated with the microwave-assisted thermal processing, similar to CS330.

In the classical CDots, photon-harvesting is due entirely to optical absorptions of the core CNPs. Upon photoexcitation, there are rapid charge transfers and separation for the formation of electrons and holes that are trapped at abundant surface defect sites of the CNPs. The separated redox pairs in the core CNPs of CDots are stabilized by the surface organic functionalization in the dots, and thus are longer lived than those in "naked" CNPs, but still highly reactive in terms of their substantial contributions to the observed antimicrobial activities of light-activated CDots [7,12,13]. The radiative recombinations of the separated redox pairs result in the emissive excited states [1], which are responsible for the observed characteristic fluorescence emissions of CDots and the generation of traditional reactive oxygen species (ROS, similar to those associated with organic photosensitizers). Thus, the potent antimicrobial function of CDots is due to the combination of the two types of reactive species: the separated redox pairs and the ROS [7,11,12]. For the former, their short-lived nature (shorter than the upper limit of diffusion in solution) generally requires near-neighbor interactions for the antimicrobial action, namely the core CNPs in CDots or the nano-carbon domains in the carbonization-produced samples, and their targeted microbial species must be in the very close proximity (thus, there is no need for any diffusion). In fact, previous studies have demonstrated that the antimicrobial action of the separated redox pairs could not be "quenched" by classical ROS scavengers [7,12,13].

Nevertheless, several experiments have confirmed that the classical scavengers can protect the targeted bacterial species from the ROS generated in the emissive excited states of CDots [7,12,13]. Such a mechanistic framework is also applicable to the hybrid samples that are prepared with processing conditions for sufficient carbonization (CS330 and CS_{MT}).

In this regard, we also examined the total ROS levels generated by the different hybrid samples with light activation during the treatment of VSVs. Figure 3 shows the fold increases of generated ROS by the different hybrid samples relative to that in the VSVs without dots treatment. As expected, the ROS levels generated in the VSVs samples treated with CS330 and CS_{MT} at 50 or 100 µg/mL were increased by ~7–15 folds relative to those in VSVs samples without dots treatment, and the increase was similar to that in the PEI-CDots treated samples, whereas there was almost no increase in ROS generation in the VSVs samples treated with CS200. The results are generally consistent with those related to the antiviral activity of the same hybrid samples shown in Figure 2. Clearly, the hybrid samples of more nano-carbon contents (CS330 and CS_{MT}) are capable of generating increased levels of ROS to contribute to the observed antiviral outcome, but not the CS200 sample. This again suggests that the effectiveness of photoinduced antiviral function of the hybrid samples is correlated with the content of the carbonization-produced nano-carbon domains in the samples, which are responsible for the absorption of visible photons to generate the reactive species. However, it should be pointed out that the relative magnitudes of increases in ROS among these samples and between different concentrations of the same sample are not exactly correlated with the order of the relative antiviral effectiveness. This may be explained by considering that the ROS generated in the emissive excited states is only one of the two contributors to the observed antiviral activities. The other contributor is the short-lived redox pairs discussed above, though the experimental quantification of the contribution remains a major challenge due to the intrinsically difficult and costly nature of ultrafast time-resolved spectroscopy techniques. Nevertheless, there is indirect experimental evidence of the involvement of the separated redox pairs based on the published results [38] on the quenching of fluorescence emission intensities of CS330 and CS_{MT} by both electron donor *N,N*-diethylaniline (DEA) and electron acceptor 2,4-dinitrotoluene (DNT). Regardless of the mechanistic details, there are clear correlations between the photoexcited state generation of reactive species and the degree of carbonization (or the content of nano-carbon domains) in the hybrid samples, and their photoinduced antiviral activities.

Figure 3. The fold increases in the total ROS generation in VSVs upon the treatments with 50 and 100 µg/mL of CS200, CS330, CS_{MT} and PEI-CDots, with 1 h visible light exposure, relative to the ROS in VSVs without dots treatment.
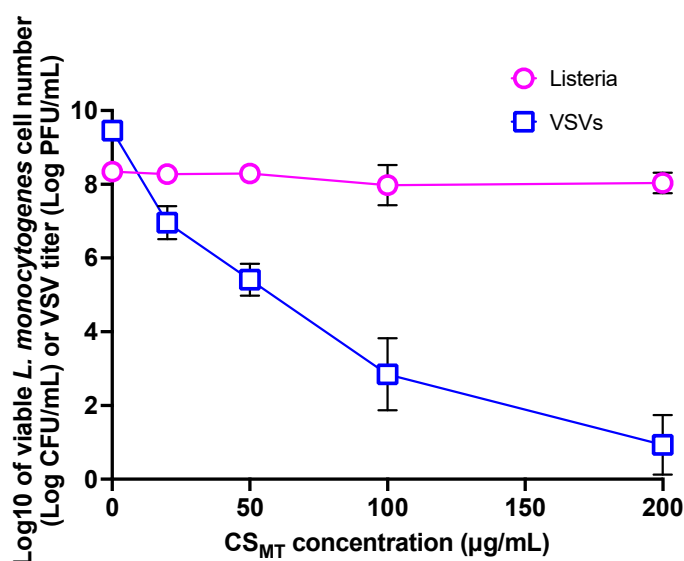
On the structure of carbonization-produced samples, the nano-carbon domains are immersed in the matrix of organic species, which is equivalent to the configuration locally of each CNP-like entity with organic passivation, thus adhering to the definition of CDots [1]. Such equivalency may be responsible for the observed antimicrobial properties of hybrid samples, except for those samples (e.g., CS200) containing small nano-carbon domains due to insufficient carbonization in their syntheses (Representative AFM image of CS200 is provided in Supplementary Materials Figure S2) [48]. On the other hand, the equivalency made possible by the local configuration in hybrid samples may not guarantee the same antimicrobial activities as those of classical CDots, including the difference between antibacterial and antiviral activities. One such case is the divergence exhibited by the CS_{MT} sample with light activation against bacteria [48] versus viruses.

3.3. Divergence in CS_{MT}'s Antiviral and Antibacterial Activities

The antiviral activities of the hybrid samples CS200 and CS330 prepared via thermal carbonization of the CA–PEI mixture as precursor are mostly in the same order as the antibacterial activities observed and reported previously [48], but not those of the CS_{MT} sample. As compared in Figure 4, the CS_{MT} sample exhibited significant antiviral function towards VSVs, but no antibacterial function towards *Listeria* cells. Interestingly, CS_{MT} exhibited its antiviral activity very similarly to CS330 (Figure 2), but its antibacterial activity is completely different from that of CS330 [48]. Our earlier study suggested no major differences in the photoexcited state redox characteristics and the optical properties between CS330 and CS_{MT}, including their similarly characteristic excitation wavelength-dependent fluorescence emissions, and similar results in the redox quenching of fluorescence emissions with electron donor *N*,*N*-diethylaniline (DEA) and acceptor 2,4-dinitrotoluene (DNT) as quenchers [48]. The divergence between CS_{MT}'s antiviral and antibacterial activities and the difference from the CS330 sample suggest that there must be other important factors besides the content of nano-carbon domains governing the photoinduced antimicrobial properties. Among the likely factors are the structural and morphological characteristics of the hybrid samples that could affect the interactions of the nano-carbon domains in the dot samples with the targeted microbial species.

As discussed above in the mechanistic framework for the antimicrobial function of light-activated CDots or hybrids, the separated redox pairs provide a major contribution to the antimicrobial outcome. However, since their contribution requires near-neighbor interactions with the targeted microbial species, it must be particularly sensitive to the structural and morphological characteristics of the dot sample. In CS_{MT} and CS330, both have significant contents of nano-carbon domains, which are immersed in and likely crosslinked with abundant organic species that survived the carbonization processing conditions, resulting in a porous sponge-like sample structure. Consequently, the interactions with the microbial species are sensitive to the spongy morphology, which might be different between CS_{MT} and CS330. In the former, the pores' size and configuration are probably inadequate for the required interactions with the larger-sized bacteria cell (*L. monocytogenes* 0.5–4 μm in diameter × 0.5–2 μm in length [52]) but sufficient for the smaller-sized virus particle (VSV 70 × 200 nm [53,54]); namely, the structural and morphological characteristics of CS_{MT} are such that they are unfavorable to the larger-sized bacterial cells but suitable for the smaller-sized virus particles. The AFM imaging results of CS_{MT} and CS330 samples [48] (Supplementary Materials, Figure S2) seem consistent with the argument about their structural and morphological differences. However, more quantitative and systematic morphological characterizations of the different hybrid samples in further investigations are needed to achieve an in-depth understanding of the interactions between the hybrid samples and the target microbials and the detailed action of their photoinduced antimicrobial activities.

Figure 4. The dose-dependent antiviral activity (to VSVs) and antibacterial activity (to *Listeria monocytogenes*) of CS_{MT}, with 1 h visible-light exposure, expressed by the reduction in $\log_{10}$ of viral titers or viable cell numbers with increasing concentrations of CS_{MT} used in the treatments.

4. Summary and Conclusions

The results reported here clearly demonstrate the divergence in photoinduced antiviral activities between the nano-carbon/organic hybrids created via thermal processing of PEI and citric acid mixtures as precursors and the classical CDots made from pre-existing carbon nanoparticles surface functionalized by PEI, with the latter exhibiting significantly better antiviral activity. The divergence is most likely correlated with the extent of carbonization in the hybrid samples, and also largely influenced by the resulting sample structural and morphological differences. Obviously, CS200 contains little nano-carbon due to the processing conditions being too mild for meaningful carbonization. For the more appropriately prepared CS330 and CS_{MT}, they are both structurally equivalent to small or tiny carbon dots crosslinked by a significant amount of organic species that survived the carbonization processing conditions, and thus are morphologically different from the mostly individual dots in the PEI-CDots sample. While both CS330 and CS_{MT} may be viewed as similar to porous composites like ("hybrids"), there are still differences. The CS_{MT} sample is apparently more discriminative in its interaction with microbials of different sizes, allowing the smaller-sized virus particles to come into closer contact with the nano-carbon domains in the sample, while the same is not true for larger-sized bacterial cells. Overall, the reported findings strongly suggest that the content of nano-carbon domains in the carbonization-prepared hybrid samples is the key component that is responsible for the photoinduced antimicrobial activity, and further, the subtle nanoscale or sub-nanoscale structural and morphological features in the carbonization-produced samples play an important role in enabling or hindering the lethal action of the highly reactive species produced in the photoexcited states of carbon dots or nano-carbon domains. Both features are required to make the hybrid samples effective in their photoinduced antimicrobial performance. The results reported here may have broad implementations, as there are a large number of dot samples synthesized by using various organic precursors under different thermal carbonization conditions, which are often considered in the literature as "carbon dots" without enough concerns for their different sample structures and properties, among themselves and especially in comparison with those of the classical CDots, and for the consequences of such differences. The obvious divergences demonstrated in this work on the antimicrobial activities of the different samples should serve as a reminder when pursuing many applications, including antimicrobial uses and others. Based on the results of the tested dot platforms, it is clear that carbon dots classically synthesized with the use

of pre-existing small carbon nanoparticles are superior to carbonization produced nano-carbon/organic hybrids in terms of their light-activated antimicrobial applications [55]. Nevertheless, another important purpose of this work is to stimulate the research community's interest in joining the effort to examine more sample platforms, aiming toward a more generalized understanding of the divergences between the carbonization-produced nano-carbon/organic hybrids and the classical CDots.

Supplementary Materials: The following supporting information can be downloaded at: https://www.mdpi.com/article/10.3390/c9030079/s1. Details on the preparation of hybrids and PEI-CDots samples, VSV virus preparation and purification, Section S1: Synthesis of CS200, CS330, and CS$_{MT}$ samples; Section S2: Preparation of PEI-CDots; Section S3: VSV Virus Propagation and Purification; Figure S1: The relative antibacterial activities of PEI-CDots, CS200, CS330, and CS$_{MT}$; Figure S2: AFM images of CS200, CS330 and CS$_{MT}$ Samples.

Author Contributions: Data acquisition and analyses, C.E.R., A.F.A., B.S. and S.Y.; Funding acquisition, L.Y., Y.T. and Y.-P.S.; Investigation, C.E.R., A.F.A., B.S. and S.Y.; Project administration, L.Y. Y.T. and Y.-P.S.; Supervision, L.Y. and Y.-P.S.; Validation, A.F.A.; Writing—original draft, L.Y. and Y.-P.S.; Writing—review and editing, Y.T., L.Y. and Y.-P.S. All authors have read and agreed to the published version of the manuscript.

Data Availability Statement: All data are contained within the article or Supplementary Materials.

Conflicts of Interest: The authors declare no conflict of interest.

References

1. Sun, Y.-P. *Carbon Dots—Exploring Carbon at Zero-Dimension*; Springer International Publishing: New York, NY, USA, 2020.
2. Sun, Y.-P.; Zhou, B.; Lin, Y.; Wang, W.; Fernando, K.A.S.; Pathak, P.; Meziani, M.J.; Harruff, B.A.; Wang, X.; Wang, H.; et al. Quantum-Sized Carbon Dots for Bright and Colorful Photoluminescence. *J. Am. Chem. Soc.* **2006**, *128*, 7756–7757. [CrossRef]
3. Sun, Y.-P. Fluorescent Carbon Nanoparticles. U.S. Patent 7,829,772, 9 November 2010.
4. Meziani, M.J.; Dong, X.; Zhu, L.; Jones, L.P.; LeCroy, G.E.; Yang, F.; Wang, S.; Wang, P.; Zhao, Y.; Yang, L.; et al. Visible-Light-Activated Bactericidal function of carbon dots "Quantum" dots. *ACS Appl. Mater. Interfaces* **2016**, *8*, 10761–10766. [CrossRef]
5. Al Awak, M.M.; Wang, P.; Wang, S.; Tang, Y.; Sun, Y.P.; Yang, L. Correlation of carbon dots' light-activated antimicrobial activities and fluorescence quantum yield. *RSC Adv.* **2017**, *7*, 30177–30184. [CrossRef]
6. Dong, X.; Overton, C.M.; Tang, Y.; Darby, J.P.; Sun, Y.-P.; Yang, L. Visible light-activated carbon dots for inhibiting biofilm formation and inactivating biofilm-associated bacterial cells. *Front. Bioeng. Biotechnol.* **2021**, *9*, 786077. [CrossRef]
7. Dong, X.; Ge, L.; Abu Rabe, D.I.; Mohammed, O.O.; Wang, P.; Tang, Y.; Kathariou, S.; Yang, L.; Sun, Y.-P. Photoexcited state properties and antibacterial activities of carbon dots relevant to mechanistic features and implications. *Carbon* **2020**, *170*, 137–145. [CrossRef]
8. Dong, X.; Liang, W.; Meziani, M.J.; Sun, Y.-P.; Yang, L. Carbon dots as potent antimicrobial agents. *Theranostics* **2020**, *10*, 671–686. [CrossRef]
9. Abu Rabe, D.I.; Al Awak, M.M.; Yang, F.; Okonjo, P.A.; Dong, X.; Teisl, L.R.; Wang, P.; Tang, Y.; Pan, N.; Sun, Y.-P.; et al. The dominant role of surface functionalization in carbon dots' photo-activated antibacterial activity. *Int. J. Nanomed.* **2019**, *14*, 2655–2665. [CrossRef]
10. Abu Rabe, D.I.; Mohammed, O.O.; Dong, X.; Patel, A.K.; Overton, C.M.; Tang, Y.; Kathariou, S.; Sun, Y.P.; Yang, L. Carbon dots for highly effective photodynamic inactivation of multidrug-resistant bacteria. *Mater. Adv.* **2020**, *1*, 321–325.
11. Dong, X.; Wang, P.; Darby, J.P.; Tang, Y.; Overton, C.M.; Kathariou, S.; Sun, Y.-P.; Yang, L. Photoactivated carbon dots for inactivation of foodborne pathogens *Listeria* and *salmonella*. *Appl. Environ. Microbiol.* **2021**, *87*, e0104221. [CrossRef]
12. Dong, X.; Edmondson, R.; Yang, F.; Tang, Y.; Wang, P.; Sun, Y.-P.; Yang, L. Carbon dots for effective photodynamic inactivation of virus. *RSC Adv.* **2020**, *10*, 33944–33954. [CrossRef]
13. Adcock, A.F.; Wang, P.; Ferguson, I.S.; Obu, S.C.; Sun, Y.-P.; Yang, L. Inactivation of Vesicular Stomatitis Virus with Light-Activated Carbon Dots and Mechanistic Implications. *ACS Appl. Bio Mater.* **2022**, *5*, 3158–3166. [CrossRef] [PubMed]
14. Dong, X.; Moyer, M.M.; Yang, F.; Sun, Y.-P.; Yang, L. Carbon Dots' Antiviral Functions against Noroviruses. *Sci. Rep.* **2017**, *7*, 519. [CrossRef] [PubMed]
15. Luo, P.G.; Sahu, S.; Yang, S.-T.; Sonkar, S.K.; Wang, J.; Wang, H.; LeCroy, G.E.; Cao, L.; Sun, Y.-P. Carbon "Quantum" Dots for Optical Bioimaging. *J. Mater. Chem. B* **2013**, *1*, 2116–2127. [CrossRef]

16. Ding, C.; Zhu, A.; Tian, Y. Functional Surface Engineering of C-Dots for Fluorescent Biosensing and in Vivo Bioimaging. *Acc. Chem. Res.* **2014**, *47*, 20–30. [CrossRef] [PubMed]

17. Luo, P.G.; Yang, F.; Yang, S.-T.; Sonkar, S.K.; Yang, L.; Broglie, J.J.; Liu, Y.; Sun, Y.-P. Carbon-Based Quantum Dots for Fluorescence Imaging of Cells and Tissues. *RSC Adv.* **2014**, *4*, 10791–10807. [CrossRef]

18. Lim, S.Y.; Shen, W.; Gao, Z. Carbon Quantum Dots and Their Applications. *Chem. Soc. Rev.* **2015**, *44*, 362–381.

19. Fernando, K.A.S.; Sahu, S.; Liu, Y.; Lewis, W.K.; Guliants, E.A.; Jafariyan, A.; Wang, P.; Bunker, C.E.; Sun, Y.-P. Carbon Quantum Dots and Applications in Photocatalytic Energy Conversion. *ACS Appl. Mater. Interfaces* **2015**, *7*, 8363–8376. [CrossRef]

20. LeCroy, G.E.; Yang, S.-T.; Yang, F.; Liu, Y.; Fernando, K.A.S.; Bunker, C.E.; Hu, Y.; Luo, P.G.; Sun, Y.-P. Functionalized Carbon Nanoparticles: Syntheses and Applications in Optical Bioimaging and Energy Conversion. *Coord. Chem. Rev.* **2016**, *320*, 66–81. [CrossRef]

21. Peng, Z.; Han, X.; Li, S.; Al-Youbi, A.O.; Bashammakh, A.S.; El-Shahawi, M.S.; Leblanc, R.M. Carbon Dots: Biomacromolecule Interaction, Bioimaging and Nanomedicine. *Coord. Chem. Rev.* **2017**, *343*, 256–277.

22. Hutton, G.A.M.; Martindale, B.C.M.; Reisner, E. Carbon Dots as Photosensitisers for Solar-Driven Catalysis. *Chem. Soc. Rev.* **2017**, *46*, 6111–6123. [CrossRef]

23. Xu, D.; Lin, Q.; Chang, H.-T. Recent Advances and Sensing Applications of Carbon Dots. *Small Methods* **2020**, *4*, 1900387. [CrossRef]

24. Das, R.; Bandyopadhyay, R.; Pramanik, P. Carbon Quantum Dots from Natural Resource: A Review. *Mater. Today Chem.* **2018**, *8*, 96–109. [CrossRef]

25. Du, J.; Xu, N.; Fan, J.; Sun, W.; Peng, X. Carbon Dots for In Vivo Bioimaging and Theranostics. *Small* **2019**, *15*, 1805087. [CrossRef]

26. Li, Y.; Xu, X.; Wu, Y.; Zhuang, J.; Zhang, X.; Zhang, H.; Lei, B.; Hu, C.; Liu, Y. A Review on the Effects of Carbon Dots in Plant Systems. *Mater. Chem. Front.* **2020**, *4*, 437–448. [CrossRef]

27. Indriyati; Primadona, I.; Permatasari, F.A.A.; Irham, M.A.; Nasir, D.E.M.; Iskandar, F. Recent Advances and Rational Design Strategies of Carbon Dots towards Highly Efficient Solar Evaporation. *Nanoscale* **2021**, *13*, 7523–7532. [CrossRef] [PubMed]

28. Đorđević, L.; Arcudi, F.; Cacioppo, M.; Prato, M.A. Multifunctional Chemical Toolbox to Engineer Carbon Dots for Biomedical and Energy Applications. *Nat. Nanotech.* **2022**, *17*, 112–130. [CrossRef] [PubMed]

29. Yuan, D.; Wang, P.; Yang, L.; Quimby, J.L.; Sun, Y.-P. Carbon "Quantum" Dots for Bioapplications. *Exp. Biol. Med.* **2022**, *247*, 300–309. [CrossRef]

30. Cui, L.; Ren, X.; Sun, M.; Liu, H.; Xia, L. Carbon Dots: Synthesis, Properties and Applications. *Nanomaterials* **2021**, *11*, 3419. [CrossRef]

31. He, C.; Xu, P.; Zhang, X.; Long, W. The synthetic strategies, photoluminescence mechanisms and promising applications of carbon dots: Current state and future perspective. *Carbon* **2022**, *186*, 91. [CrossRef]

32. Behi, M.; Gholami, L.; Naficy, S.; Palomba, S.; Dehghani, F. Carbon dots: A novel platform for biomedical applications. *Nanoscale Adv.* **2022**, *4*, 353. [CrossRef]

33. Dong, Y.; Wang, R.; Li, G.; Chen, C.; Chi, Y.; Chen, G. Polyamine-Functionalized Carbon Quantum Dots as Fluorescent Probes for Selective and Sensitive Detection of Copper Ions. *Anal. Chem.* **2012**, *84*, 6220–6224. [CrossRef] [PubMed]

34. Dong, Y.; Wang, R.; Li, H.; Shao, J.; Chi, Y.; Lin, X.; Chen, G. Polyamine-Functionalized Carbon Quantum Dots for Chemical Sensing. *Carbon* **2012**, *50*, 2810–2815. [CrossRef]

35. Wang, R.; Li, G.; Dong, Y.; Chi, Y.; Chen, G. Carbon Quantum Dot-Functionalized Aerogels for NO_2 Gas Sensing. *Anal. Chem.* **2013**, *85*, 8065–8069. [CrossRef] [PubMed]

36. Dong, Y.; Wang, R.; Tian, W.; Chi, Y.; Chen, G. "Turn-on" Fluorescent Detection of Cyanide Based on Polyamine-Functionalized Carbon Quantum Dots. *RSC Adv.* **2014**, *4*, 3685–3689. [CrossRef]

37. Liu, J.; Liu, X.; Luo, H.; Gao, Y. One-Step Preparation of Nitrogen-Doped and Surface-Passivated Carbon Quantum Dots with High Quantum Yield and Excellent Optical Properties. *RSC Adv.* **2014**, *4*, 7648. [CrossRef]

38. Wang, C.; Xu, Z.; Zhang, C. Polyethyleneimine-Functionalized Fluorescent Carbon Dots: Water Stability, PH Sensing, and Cellular Imaging. *ChemNanoMat* **2015**, *1*, 122–127. [CrossRef]

39. Pierrat, P.; Wang, R.; Kereselidze, D.; Lux, M.; Didier, P.; Kichler, A.; Pons, F.; Lebeau, L. Efficient in Vitro and in Vivo Pulmonary Delivery of Nucleic Acid by Carbon Dot-Based Nanocarriers. *Biomaterials* **2015**, *51*, 290–302. [CrossRef]

40. Yuan, T.; Meng, T.; He, P.; Shi, Y.; Li, Y.; Li, X.; Fan, L.; Yang, S. Carbon quantum dots: An emerging material for optoelectronic applications. *J. Mater. Chem. C* **2019**, *7*, 6820. [CrossRef]

41. Qu, D.; Sun, Z. The formation mechanism and fluorophores of carbon dots synthesized via a bottom-up. *Mater. Chem. Front.* **2020**, *4*, 400. [CrossRef]

42. Yuan, T.; Meng, T.; Shi, Y.; Song, X.; Xie, W.; Li, Y.; Li, X.; Zhang, Y.; Fan, L. Toward phosphorescent and delayed fluorescent carbon quantum dots for next-generation electroluminescent displays. *J. Mater. Chem. C* **2022**, *10*, 2333. [CrossRef]

43. Yang, X.; Ai, L.; Yu, J.; Waterhouse, G.I.; Sui, L.; Ding, J.; Zhang, B.; Yong, X.; Lu, S. Photoluminescence mechanisms of red-emissive carbon dots derived from non-conjugated molecules. *Sci. Bull.* **2022**, *67*, 1450. [CrossRef]

44. Wang, B.; Wei, Z.; Sui, L.; Yu, J.; Zhang, B.; Wang, X.; Feng, S.; Song, H.; Yong, X.; Tian, Y.; et al. Electron–phonon coupling-assisted universal red luminescence of o-phenylenediamine-based carbon dots. *Light Sci. Appl.* **2022**, *11*, 172. [CrossRef] [PubMed]

45. Pan, L.; Sun, S.; Zhang, A.; Jiang, K.; Zhang, L.; Dong, C.; Huang, Q.; Wu, A.; Lin, H. Truly Fluorescent Excitation-Dependent Carbon Dots and Their Applications in Multicolor Cellular Imaging and Multidimensional Sensing. *Adv. Mater.* **2015**, *27*, 7782. [CrossRef]

46. Sun, S.; Zhang, L.; Jiang, K.; Wu, A.; Lin, H. Toward High-Efficient Red Emissive Carbon Dots: Facile Preparation, Unique Properties, and Applications as Multifunctional Theranostic Agents. *Chem. Mater.* **2016**, *28*, 8659. [CrossRef]

47. Wang, P.; Meziani, M.J.; Fu, Y.; Bunker, C.E.; Hou, X.; Yang, L.; Msellek, H.; Zaharias, M.; Darby, J.P.; Sun, Y.-P. Carbon Dots versus Nano-Carbon/Organic Hybrids—Dramatically Different Behaviors in Fluorescence Sensing of Metal Cations with Structural and Mechanistic Implications. *Nanoscale Adv.* **2021**, *3*, 2316–2324. [CrossRef] [PubMed]

48. Adcock, A.F.; Wang, P.; Cao, E.Y.; Ge, L.; Tang, Y.; Ferguson, I.S.; Abu Sweilem, F.S.; Petta, L.; Cannon, W.; Yang, L.; et al. Carbon Dots versus Nano-Carbon/Organic Hybrids—Divergence between Optical Properties and Photoinduced Antimicrobial Activities. *C* **2022**, *8*, 54. [CrossRef]

49. Hu, Y.; Al Awak, M.M.; Yang, F.; Yan, S.; Xiong, Q.; Wang, P.; Tang, Y.; Yang, L.; LeCroy, G.E.; Bunker, C.E.; et al. Photoexcited State Properties of Carbon Dots from Thermally Induced Functionalization of Carbon Nanoparticles. *J. Mater. Chem. C* **2016**, *4*, 10554–10561. [CrossRef]

50. Ge, L.; Pan, N.; Jin, J.; Wang, P.; LeCroy, G.E.; Liang, W.; Yang, L.; Teisl, L.R.; Tang, Y.; Sun, Y.-P. Systematic Comparison of Carbon Dots from Different Preparations—Consistent Optical Properties and Photoinduced Redox Characteristics in Visible Spectrum, and Structural and Mechanistic Implications. *J. Phys. Chem. C* **2018**, *122*, 21667–21676. [CrossRef]

51. Hou, X.; Hu, Y.; Wang, P.; Yang, L.; Al Awak, M.M.; Tang, Y.; Twara, F.K.; Qian, H.; Sun, Y.-P. Modified Facile Synthesis for Quantitatively Fluorescent Carbon Dots. *Carbon* **2017**, *122*, 389–394. [CrossRef]

52. Jamshidi, A.; Zeinali, T. Significance and Characteristics of Listeria monocytogenes in poultry products. *Int. J. Food Sci.* **2019**, *2019*, 7835253. [CrossRef]

53. Ge, P.; Tsao, J.; Schein, S.; Green, T.J.; Luo, M.; Zhou, Z.H. Cryo-EM model of the bullet-shaped vesicular stomatitis virus. *Science* **2010**, *327*, 689–693. [CrossRef] [PubMed]

54. Cureton, D.K.; Massol, R.H.; Whelan, S.P.J.; Kirchhausen, T. The Length of Vesicular Stomatitis virus Particles Dictates a Need for Actin Assembly during Clathrin-Dependent Endocytosis. *PLoS Pathog.* **2010**, *6*, e1001127. [CrossRef] [PubMed]

55. Liang, W.; Sonkar, S.K.; Saini, D.; Sheriff, K.; Singh, B.; Yang, L.; Wang, P.; Sun, Y.-P. Carbon Dots: Classically Defined versus Organic Hybrids on Shared Properties, Divergences, and Myths. *Small* **2023**, *19*, 2206680. [CrossRef] [PubMed]